A STUDY OF SOLAR EVOLUTION

D. Ezer and A.G.W. Cameron

Institute for Space Studies
Goddard Space Flight Center, NASA
New York, New York

Abstract

Evolutionary sequences of solar models have been calculated using the Henyey method of model construction. These sequences were started at the threshold of stability, at which the released gravitational potential energy of the sun is just sufficient to supply the thermal, dissociation, and ionization energies of the model. It was found that the present solar characteristics were closely reproduced when a mixing length equal to two pressure scale heights was used in the convection theory, and when a solar initial helium abundance was chosen based on solar cosmic ray measurements. The sun was again found to have a high luminosity during its contraction phase and to approach the main sequence in only a few million years. Tables of selected characteristics of some of the models are presented.

Introduction

It has been established that stars undergoing gravitational contraction to the main sequence follow a nearly vertical track in the Hertzsprung-Russell diagram (Hayashi, 1961; Ezer and Cameron, 1963; Weymann and Moore, 1963). This early evolution of the sun plays an important role in studies of the origin, structure and history of the solar system.

Preceding this early evolutionary phase is the collapse of a primordial gas cloud from the interstellar medium which requires detailed hydrodynamic considerations including the conservation of angular momentum, the influence of interstellar magnetic fields and external gravitational fields. This collapse will continue until the released gravitational potential energy of the gas cloud becomes larger than the energy required for storage as internal energy, dissociation and ionization of molecules and atoms, and energy loss from the interior. This early collapse phase of the sun has been studied by Cameron (1962).

In the present study, the construction of solar models starts from the point where the collapsing protosun becomes

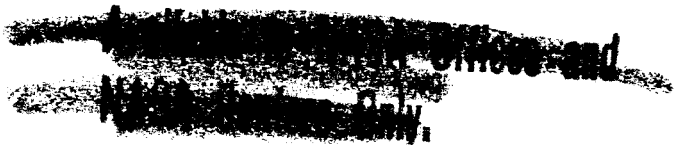

stable against further dynamical collapse. The authors previously studied the early evolution of the sun under the assumption of homologous contraction (Ezer and Cameron, 1963). A series of models, each corresponding to a definite radius, was obtained by a classical fitting method using the luminosity L, central pressure P_c, central temperature T_c, and a contraction parameter (defined below) as adjustable parameters. It was found that the collapsing protosun becomes stable, from simple energy principles, at a radius of 57 $R_\odot$. At this radius the gravitational energy, $E_{grav} = -G\int_0^M \frac{M_r dM_r}{r}$, just becomes, in absolute amount, larger than the thermal, ionization, and dissociation energies of the model star. During subsequent contraction the energy radiated from the star during a certain time interval is given by the change of gravitational and internal energy during this time interval.

In our previous study each model was constructed under the assumption of homologous contraction. In order to evaluate the evolutionary time scale, it was assumed that these models formed an evolutionary sequence. This gave a reasonable path in the luminosity-surface temperature diagram for the contracting phase, but it also caused us

to neglect the gravitational potential energy release associated with changes in the characteristic structure of the star, and in particular with the central condensation which occurs when the completely convective model changes to a largely radiative model. Consequently the contraction times previously estimated are too small.

The Henyey method of stellar model construction has been adopted for the present evolutionary study. In this method, the time-dependent non-linear differential equations governing the stellar structure are replaced by finite-difference equations, and the spatial and time differential operators by appropriate difference operators. These equations are solved simultaneously by an iterative process. Detailed descriptions of the method are given by Henyey, Forbes and Gould (1963) and by Hofmeister, Kippenhahn and Weigert (1964).

The evolutionary development of the sun must start with an initial (t = 0) model. In this investigation, the zero-time model, from which the time increase defines the structure of the subsequent model, has been obtained from the following consideration. Let us assume that the sun contracts homologously at a radius R; then the energy

balance equation can be written as

$$\frac{\partial L_r}{\partial M_r} = \left\{ - T \frac{\partial E}{\partial T} - 3 \rho \left(\frac{\partial E}{\partial \rho} - \frac{P}{\rho^2} \right) \right\} \frac{1}{R} \frac{\partial R}{\partial t}$$

where L_r is the energy crossing the surface of a sphere of radius r per second, M_r is the mass within a sphere of radius r, T is the temperature, E is the internal energy per gram of material, ρ is the density and P is the total pressure. This equation involves time only in the term $\frac{1}{R} \frac{\partial R}{\partial t}$ which is the rate of contraction to the radius R and can be written as

$$- \frac{1}{R} \frac{\partial R}{\partial t} = \mathcal{J} \frac{LR}{GM^2}$$

This expresses the contraction rate as a function of the ratio of the luminosity to the gravitational potential energy. The quantity $\mathcal{J}$ can be called the contraction parameter; it was one of the parameters that was adjusted in our previous study in order to obtain consistent solar models. $\mathcal{J}$ does not vary rapidly in a region where change in R is small. It has a value of 2.58 for the model which first becomes stable against gravitational collapse in our previous calculation. This value of $\mathcal{J}$ can be used to

fix the radius of the initial model for the present method which is assumed to contract to that radius homologously. The procedure we followed in order to obtain the initial model is explained, in detail, under the section Method of Computation.

Chemical Composition and Opacity

A preliminary evolutionary study was carried out with the same technique described in this paper and with the solar composition used in the previous homologous model construction, in which hydrogen is $X_1 = 0.602$, helium $Y_4 = 0.376$ and heavy elements $Z = 0.022$ by mass; this gave the evolutionary tracks shown in Figure 1 (Ezer and Cameron, 1964). Calculations were performed for two assumed ratios of mixing-length to pressure scale height. After an evolution time of 4.5×10^9 years, about the right radius could be obtained, but all luminosities were too high. In radiative equilibrium, which is the case for the late evolutionary models, the luminosity varies approximately as $L \propto \mu^{7.5}$. Low luminosities can thus be obtained by assuming a lower value for the above helium

content, which is based on the N/He ratio in O and B stars.

Recently Biswas, Fichtel, Guss and Waddington (1963) measured the relative abundances of He, C, N, O and Ne in solar cosmic rays in a rocket flight. The rocket results for He and Ne are of great interest since the abundance of these elements in the Sun cannot be determined spectroscopically. Gaustad (1963) gives $\frac{He}{C+N+O} = 54 \pm 6$ (p.e.) as a weighted average of the individual determinations from the rocket data of Biswas et al. The rocket cosmic ray Ne/O ratio is 0.1.

Using these relative abundances and the H:O:Si ratio in the Sun (Aller, 1963) we obtained abuncances of 2.62×10^9 for helium and 2.9×10^6 for neon relative to silicon = 10^6. Other elemental abundances were assumed as given by Ezer and Cameron (1963). These abundances give for hydrogen, $X_1 = 0.739$, for helium, $X_4 = 0.240$, and for heavy elements, $Z = 0.021$, by mass, for the initial composition of the Sun. The initial abundances of C^{12}, N^{14} and O^{16} are $X_{12} = 4.618 \times 10^{-3}$, $X_{14} = 0.97 \times 10^{-3}$ and $X_{16} = 1.0715 \times 10^{-2}$, respectively. This is the composition used for the present study.

Opacities, including line corrections, for temperature-density combinations characteristic of the solar interior with the above initial composition were kindly made available to us by A. N. Cox at Los Alamos. A second set of opacities was provided at higher densities and temperatures

for a composition in which the hydrogen had been converted into helium. Because the Los Alamos opacity code cannot handle more than at most a dozen elements simultaneously, it was necessary to group various elements together and to characterize them by a single representative element. The abundances and characteristic elements chosen are given in Table I.

Table I

Abundances of Selected Elements

Element	Mass Fraction	Element	Mass Fraction	Element	Mass Fraction
H	0.739	Na	0.91×10^{-4}	Ca	0.670×10^{-4}
He	0.240	Si	1.677×10^{-3}	Fe	1.096×10^{-3}
C	5.57×10^{-3}	Ar	2.210×10^{-4}		
O	1.205×10^{-2}	K	0.030×10^{-4}		

It should be noted that potassium was included as a separate element, uncombined with others, owing to its important role as the principal supplier of free electrons at lower temperatures. The next most important electron supplier, sodium, is combined with aluminum. It is these electrons which form

negative hydrogen ions, which give the principal contribution to the opacity at lower temperatures. The detailed results of this paper are quite sensitive to these lower temperature opacities.

Opacity tables for both the initial and hydrogen-exhausted compositions were stored in the computer, interpolation being made logarithmically. For cases of partial hydrogen exhaustion a linear interpolation (in hydrogen content) was made between the two opacity tables. Cox (1964) has shown that linear interpolation is well justified at higher temperatures.

Energy Generation

For models in the gravitational contraction phase, the sole source of energy is the gravitational contraction energy, E_{grav}. The amount of gravitational contraction energy which is released at some interior point during a time dt is defined by

$$dE_{grav} = \left[- \frac{\partial E}{\partial t} - P \frac{\partial}{\partial t} \left(\frac{1}{\rho} \right) \right] dt$$

When the interior temperature increases sufficiently nuclear energy generation starts to take place. In this study energy generation by deuterium-burning, He^3-burning, the first two proton-proton chains, and the CNO bi-cycle were included.

The energy generation rate for the deuterium-burning through the $D^2(p,\gamma)He^3$ reaction is given by

$$\varepsilon_D = 6.362 \times 10^{23} X_1 X_2 \rho f_{2,1} g_{2,1} \frac{e^{-37.210/T_6^{1/3}}}{T_6^{2/3}} \text{ erg/gm-sec}$$

where T_6 is the temperature in units of 10^6 ^oK, X_1 and X_2 are the fractional hydrogen and deuterium abundances by mass, f is the electron screening factor, and g is an additional correction term. Their values for this reaction are:

$$f_{2,1} = 1 + 0.25 \rho^{1/2}/T_6^{3/2}$$

$$g_{2,1} = 1 + 1.12 \times 10^{-2} T_6^{1/3} + 3.12 \times 10^{-2} T_6^{2/3} + 2.45 \times 10^{-3} T_6$$

which are taken from Reeves (1963).

When the first proton-proton chain terminates with the formation of He^3, the energy generation rate is given by

$$\epsilon'_{1,1} = 1.06 \times 10^6 \, f_{1,1} \, g_{1,1} \, \rho \, X_1^2 \, \frac{e^{-33.810/T_6^{1/3}}}{T_6^{2/3}} \text{ erg/gm-sec}$$

with

$$f_{1,1} = 1 + 0.25 \, \rho^{1/2}/T_6^{3/2}$$

$$g_{1,1} = 1 + 1.23 \times 10^{-2} \, T_6^{1/3} + 7.80 \times 10^{-3} \, T_6^{2/3} + 6.73 \times 10^{-4} \, T_6$$

The energy generation rate for the $He^3(He^3, 2p)He^4$ reaction is

$$\epsilon_{3,3} = 8.895 \times 10^{29} \, \rho \, X_3^2 \, f_{3,3} g_{3,3} \frac{e^{-122.774/T_6^{1/3}}}{T_6^{2/3}} \text{ erg/gm-sec}$$

where X_3 is the He^3 concentration by mass and

$$f_{3,3} = 1 + \rho^{1/2}/T_6^{3/2}$$

$$g_{3,3} = 1 + 3.39 \times 10^{-3}\ T_6^{1/3}$$

He^3 reacts with whatever He^4 is present, leading to the second proton-proton chain. The energy generation rate for the $He^3(\alpha,\gamma)Be^7$ and $Be^7(e^-,\nu)Li^7(p,\gamma)Be^8 \rightarrow 2\ He^4$ reactions is given by

$$\epsilon_{3,4} = r_{3,4}\left[Q_{3,4} + \left(WQ_{7,1} + Q_{7,e}\right)\frac{1}{W+1}\right] \text{ erg/gm-sec.}$$

The reaction rate for the $He^3(\alpha,\gamma)Be^7$ reaction is

$$r_{3,4} = 2.41 \times 10^{31}\ f_{3,4}\ g_{3,6}\ \rho\ X_3\ Y_4\ \frac{e^{-128.277/T_6^{1/3}}}{T_6^{2/3}}$$

where X_4

$$f_{3,4} = 1 + 1.0\ \rho^{1/2}/T_6^{2/3}$$

$$g_{3,4} = 1 + 3.25 \times 10^{-3}\ T_6^{1/3} - 2.15 \times 10^{-3}\ T_6^{2/3} - 4.90 \times 10^{-5}\ T_6$$

W is the ratio of the Be^7 proton capture rate to the Be^7 electron capture rate and its value is

$$W = 0.613 \times 10^{16}\ X_1\ \mu_e\ f_{7,1}\ g_{7,1}\ \frac{e^{-102.645/T_6^{1/3}}}{T_6^{1/6}}$$

where μ_e is the mean molecular weight per electron, and

$$f_{7,1} = 1 + 1.0 \frac{\rho^{1/2}}{T_6^{2/3}}$$

$$g_{7,1} = 1 + 4.06 \times 10^{-3} T_6^{1/3}$$

The Be^7 proton capture rate is obtained from Reeves (1963), and the Be^7 electron capture rate is that given by Bahcall (1962). The energy liberated as a result of the fusion of the two elements in question is taken as follows:

$Q_{3,4} = 2.542 \times 10^{-6}$ erg/reaction; $Q_{7,1} = 1.748 \times 10^{-5}$ erg/reaction; $Q_{7,e} = 2.789 \times 10^{-5}$ erg/reaction.

When He^3 reaches its steady state value in the proton-proton chain, or equivalently when the destruction time of He^3 becomes smaller than the evolution time between two models, than the energy generation rate is given by the formula (Reeves, 1963)

$$\epsilon_{pp} = \epsilon' \Psi_{pp}(\alpha, W) \text{ erg/gm-sec}$$

where

$$\epsilon' = 2.06 \pm 0.2 \times 10^6 f_{1,1} g_{1,1} \rho X_1^2 \frac{e^{-33.81/T_6^{1/3}}}{T_6^{2/3}} \text{ erg/gm-sec}$$

$$\Psi_{pp}(\alpha,W) = \left[1 + \gamma\left(0.959 - \frac{0.492\ W}{1 + W}\right)\right]$$

with the following definitions:

$$\gamma = \left[\left(1 + \frac{2}{\alpha}\right)^{1/2} - 1\right]\alpha;$$

$$\alpha = 5.48 \times 10^{17}\ e^{-100/T_6^{1/3}} \left(\frac{X_4}{4X_1}\right)^2 ;$$

In the CNO bi-cycle the secondary elements N^{13}, C^{13}, O^{15}, and N^{15} are assumed to be destroyed as rapidly as they are formed. The energy generation rate by the $C^{12}(p,\gamma)N^{13}(e^+\nu)C^{13}(p,\gamma)N^{14}$ reaction is given by

$$\epsilon_{12,1} = 1.504 \times 10^{27}\ f_{12,1}\ g_{12,1}\ \rho\ X_1\ X_{12}\ \frac{e^{-136.926\ /T_6^{1/3}}}{T_6^{2/3}}$$

with

$$f_{12,1} = 1 + 1.5\ \frac{\rho^{1/2}}{T_6^{3/2}}$$

$$g_{12,1} = 1 + 3.04 \times 10^{-3}\ T_6^{1/3} + 1.90 \times 10^{-2}\ T_6^{2/3} + 4.05 \times 10^{-4}\ T_6$$

The energy generation rate by the sequence of $N^{14}(p,\gamma)O^{15}(e^+\nu)N^{15}(p,\alpha)C^{12}$ reaction is

$$\epsilon_{14,1} = 4.44 \times 10^{27} f_{14,1} g_{14,1} \rho X_1 X_{14} \frac{e^{-152.311/T_6^{1/3}}}{T_6^{2/3}}$$

where

$$f_{14,1} = 1 + 1.75 \rho^{1/2}/T_6^{3/2}$$

$$g_{14,1} = 1 + 2.74 \times 10^{-3} T_6^{1/3} - 3.74 \times 10^{-3} T_6^{2/3} - 7.17 \times 10^{-5} T_6$$

During the evolution C^{12} is depleted toward its equalibrium value with N^{14}. The energy generation by the $O^{16}(p,\gamma)F^{17}(e^{+}\nu)O^{17}(p,\alpha)N^{14}$ reaction is considered negligible, but the increase of the N^{14} abundance through this sequence has been properly taken into account throughout the evolution. When the equilibrium abundance is reached between C^{12} and N^{14} nuclei; the energy generation rate is governed by the $N^{14}(p,\gamma)O^{15}$ reaction and energy release is 2502 Mev per cycle; hence

$$\epsilon_{CNO} = 7.94 \times 10^{27} f_{14,1} g_{14,1} \rho X_1 X_{14} \frac{e^{-152.313/T_6^{1/3}}}{T_6^{2/3}}$$

Method of Computation

The method used was the newer version of the Henyey method (Henyey et al., 1964). The time dependent non-linear differential equations for stellar structure are written in the form of difference equations which involve the values of physical variables at two consecutive spatial steps within the star. Here we only explain some characteristics of our computing program which might be of interest in the application of the method.

The computing program is entirely automatic and consists of two parts, an atmospheric part and an interior part.

The equations used in each part are the same except:

(a) When the radiative temperature gradient becomes larger than the adiabatic temperature gradient

$$\left|\frac{dT}{dr}\right| > \left|\frac{dT}{dr}\right|_{ad}$$

the stability of the mass layers will be disturbed and convective motions will start. The atmospheric computation treats the mass motions of the convective elements according to the Böhm-Vitense (1958) mixing-length theory, in which the temperature gradient can be considerably superadiabatic. The radiative energy losses of the convective elements are taken into account and the mixing-length ℓ can be taken as a constant multiple of the pressure or density scale height. The equations used for the convective theory and the method of solution for obtaining the superadiabatic temperature gradient have been previously discussed by Ezer and Cameron (1963), and essentially the same procedure was followed in the present work. However, the interior computation assumes that any possible convection sets up an adiabatic temperature gradient. In each computation the adiabatic temperature gradient can be obtained for a material which is undergoing dissociation or ionization. The effect of radiation energy

and change of mean molecular weight were also included. Hydrogen and helium have each been considered in three states: H_2, H, H^+ and He, He^+, He^{++}. The equation of state allows for partial and complete non-relativistic degeneracy of the electrons and includes the radiation pressure.

(b) The energy flow equation which defines the luminosity of the star

$$\frac{dL_r}{dM_r} = \epsilon_{nuc} - \frac{\partial E}{\partial T} - P \frac{\partial}{\partial t}\left(\frac{1}{\rho}\right)$$

is simplified in the atmosphere. Energy generation by nuclear processes, ϵ_{nuc}, and by gravitational contraction has been neglected.

(c) The atmospheric computation, for a given combination of radius R and luminosity L, starts in the same way as described in Ezer and Cameron (1963). The calculations are carried out down to a certain fraction of the total mass, M_f and give a set of values of r_f, T_f, ρ_f, L_f for radius, temperature, density and luminosity which supply the boundary condition for the interior solutions. Since the Henyey method is an iterative procedure, after each iteration for the differential corrections to the pre-estimated values of L and R, a new atmosphere must be fitted. Since the most time-consuming part of the stellar evolution program is the atmospheric calculations, it is desirable to be able to interpolate r_f, ρ_f, T_f, L_f

at M_f among four previously computed atmospheres. Four sets of atmospheric calculations, each corresponding to a small increase or decrease of the values of the total luminosity L and radius R, constitute the corners of a rectangular grid. As long as R and L stay in the grid after each iteration with the differential corrections, the same rectangular grid can be used to interpolate the values of r_f, ρ_f, T_f, L_f. Otherwise a new grid must be calculated around the new L and R values.

The choice of a mass fraction down to which the atmospheric calculations will be performed depends on the nature of the model in question. First of all, at the end of the atmospheric calculations, the temperature gradient should be close to its adiabatic value, if convection is present. The surface conditions play a very important role in determining the evolution of the star with low surface temperatures. In the transition layers between radiative and convective equilibrium, the temperature gradient becomes extremely superadiabatic and it stays quite superadiabatic in a large portion of the outer layers of the star. Therefore, the fractional mass cannot be taken very small. On the other hand, it should not be

taken very large since energy generation by gravitational contraction has been neglected in the computation of the atmosphere. This neglect might become important for the rapidly changing models in the early gravitational contraction phases. For an accurate attainment of the adiabatic gradient in the early contraction phases we found $M_f = 0.98\ M_{total}$. Actually we found that the accuracy of the computations is much more affected by using a larger size grid around the L and R combination than by the above-mentioned approximations. In the early gravitational phases, in which the sun has large radius and high luminosity, we used an atmospheric grid for a 2% increase and decrease of the luminosity and radius. Later on, we allowed up to 10% change in the L and R radius for calculating the grid.

The remaining mass in the interior part of the star can be considered as consisting of a number of concentric shells. Each shell contains a certain fraction of the total mass and stays constant throughout the evolution. In general, it is desirable to keep the physical variables from one mass zone to the next one as smooth as possible. The number of mass zones used depends on the degree of accuracy which is desired. We selected 120 constant mass

points for the 98% of the total mass remaining in the interior of the star. Thirty-five of these were within 1% of the total mass near the center while there are only 10 zones in the 1% of the total mass near the outer fitting mass point M_f. A new zone can be inserted or a zone can be deleted by checking the increase of selected variables from one spatial step to the next. The selection of criteria for this vary considerably at the different phases of the evolution of a star. At present, we use the criteria that Henyey suggested and, with the number of mass zones that we selected, it was only necessary to insert a small number of zones.

In order to start the evolutionary calculations we proceeded in the following way. First, the energy flow equation was replaced by the one based on the assumption that contraction is homologous. The model with a radius of 57 $R_\odot$ for the contracting sun, which was obtained for homologous contraction, was our preliminary initial configuration. This model gives us approximate values for the variables r_j, T_j, ρ_j, L_j at each chosen mass point $M(j)$. The interior mass was divided into 120 mass points in the way mentioned above. Knowing the total luminosity and

radius of the 57 $R_\odot$ model, we calculated four atmospheric grid points, each corner corresponding to a 10% increase and decrease of the (L,R) combination. Now this preliminary initial model can be very easily relaxed in the Henyey method using the contraction parameter $J = 2.58$. Small corrections to r_j, ρ_j, T_j, L_j and L,R are required due to the change of method. The model can be improved by decreasing the size of the atmospheric grid. Then the stability criterion is checked by computing the gravitational energy E_{grav} and internal energy E_{in} for the model. The radius of this model can be adjusted in such a way that the difference between the total gravitational energy and the internal energy should be smaller than some desired value. If it is larger than the desired value, the radius R_o is increased by an amount C_R and small changes in the distribution of physical variables can be found by the homology transformation. The new radius $R = C_R R_o$ and, to a good approximation, the luminosity $L = C_R^2 L_o$. If $\left|\frac{E_{grav} - E_{in}}{E_{grav}}\right| < 0.03$, we considered the configuration satisfactory for the time-zero model.

In order to proceed with further evolution, first an arbitrary time step was taken. Estimated values for the

r_j, ρ_j, T_j, L_j and (L,R) for the first evolutionary model were taken as those of the zero time model, and the required differential corrections were applied by solving the variational equations in the Henyey method. In general, for later models the estimated values of the variables for a new model were obtained by extrapolation from the corresponding values of the previous models. The program can handle parabolic and linear extrapolation, whichever is desired, and the time step can be enlarged or reduced during the course of evolution entirely automatically as may be necessary.

A corrective iteration is considered to be a final one if the relative changes

$$\frac{\delta r_j}{r_j}, \frac{\delta T_j}{T_j}, \frac{\delta \rho_j}{\rho_j}, \frac{\delta L_j}{L_j}$$

become smaller than 10^{-3} for all zone boundaries. If the solutions are the real physical ones, they should satisfy the equations for stellar structure.

The radiative and adiabatic gradients are evaluated at the boundaries of a zone. These are then averaged to find the gradients for that zone. If the radiative gradient

is larger than the adiabatic in absolute value, the zone is treated as convective; otherwise it is radiative. The boundary between radiative and convective regions is obtained by interpolation in order to find the mass fraction where the difference in the gradients is zero, and temporary coincident double zone boundaries are then inserted in order to handle discontinuities in composition.

Results

This investigation was carried out to study the evolutionary changes in the structure of the sun from the time it becomes stable against gravitational collapse up to its present age. The calculations were performed for two assumed values of the ratio of mixing-length to pressure scale height, $\frac{\ell}{H}$. The results of the computations, for some selected evolutionary models, are summarized in Table 2 and Table 3 for $\frac{\ell}{H} = 1$ and 2, respectively. The first column indicates the age of the models in years. The other columns show, in turn, the radius, the luminosity, the central temperature and central density for each model. Tables 4 and 5 give the radius and luminosity of the models

TABLE 2

Evolutionary Sequence of Models

Initial Composition $X_1 = 0.739$, $Z = 0.021$, and $\frac{\ell}{H} = 1$

Age yrs.	R cm	L erg sec^{-1}	T_c ^oK	ρ_c gm cm^{-3}
3.17	4.23×10^{12}	1.29×10^{36}	1.43×10^{5}	6.76×10^{-5}
1.27×10	4.15	1.24	1.45	7.04
4.75	3.95	1.16	1.52	8.02
1.24×10^{2}	3.62	1.03	1.65	1.02×10^{-4}
3.01	3.10	8.07×10^{35}	1.90	1.52
6.56	2.56	6.01	2.28	2.54
1.16×10^{3}	2.16	4.63	2.67	4.05
2.79	1.61	2.93	3.50	9.05
5.62	1.25	1.97	4.45	1.85×10^{-3}
1.21×10^{4}	9.45×10^{11}	1.26	5.82	4.10
2.83	6.88	7.52×10^{34}	7.89	1.02×10^{-2}
7.38	4.80	4.06	1.12×10^{6}	2.88
1.26×10^{5}	3.93	2.86	1.36	5.17
2.55	3.03	1.81	1.75	1.10×10^{-1}
6.71	2.46	9.26×10^{33}	2.43	2.94
1.09×10^{6}	1.85	6.83	2.83	4.72
1.92	1.54	4.69	3.39	8.16
3.58	1.26	3.11	3.99	1.57×10^{0}
5.24	1.12	2.42	3.42	2.51
8.56	9.68×10^{10}	1.85	5.06	4.89
1.19×10^{7}	8.87	1.66	5.66	8.33
1.85	8.16	1.79	7.14	2.12×10^{1}
2.19	8.12	2.11	8.03	3.21
3.18	8.13	3.78	1.21×10^{7}	8.89
3.35	7.97	3.84	1.30	9.23
3.52	7.70	3.72	1.35	9.27
4.51	6.79	2.79	1.38	8.51
5.84	6.73	2.70	1.37	8.50
8.41	6.78	2.76	1.37	8.78
1.14×10^{8}	6.79	2.80	1.37	9.02
2.94	6.84	2.85	1.37	9.25
5.33	6.89	2.90	1.38	9.47
7.73	6.93	2.95	1.39	9.71
1.01×10^{9}	6.98	3.00	1.40	9.96
2.21	7.25	3.24	1.45	1.15×10^{2}
3.17	7.42	3.49	1.50	1.32
4.13	7.69	3.76	1.56	1.55
4.50	7.75	3.88	1.58	1.66

TABLE 3

Evolutionary Sequence of Models

Initial Composition $X_1 = 0.739$, $Z = 0.021$, and $\frac{\ell}{H} = 2$

Age yrs.	R cm.	L erg sec^{-1}	T_c ^oK	ρ gm cm^{-3}
3.17	4.47×10^{12}	2.62×10^{36}	1.37×10^{5}	6.08×10^{-5}
1.27×10	4.33	2.51	1.41	6.60
3.72	4.04	2.25	1.51	7.93
1.13×10^{2}	3.46	1.81	1.75	1.19×10^{-4}
2.15	3.02	1.44	1.98	1.71
6.20	2.23	9.00×10^{35}	2.61	3.82
1.03×10^{3}	1.95	7.20	2.96	5.48
2.44	1.45	4.54	3.90	1.24×10^{-3}
6.30	9.85×10^{11}	2.44	5.62	3.70
1.28×10^{4}	7.53	1.56	7.26	7.94
2.58	5.79	9.98×10^{34}	9.35	1.69×10^{-2}
7.12	4.00	5.29	1.34×10^{6}	5.02
1.10×10^{5}	3.38	3.78	1.58	8.08
2.66	2.50	2.18	2.13	1.98×10^{-1}
5.78	1.91	1.23	2.75	4.31
1.82×10^{6}	1.31	4.9×10^{33}	3.94	1.32×10^{0}
2.65	1.17	3.74	4.32	1.91
4.31	1.03	2.77	4.79	3.17
7.64	8.92×10^{10}	2.09	5.51	6.42
1.43×10^{7}	7.72	2.00	7.09	1.90×10^{1}
2.09	7.26	2.71	9.36	4.82
2.76	6.94	3.74	1.22×10^{7}	8.73
2.92	6.85	3.92	1.30	9.19
3.26	6.49	3.47	1.37	8.87
3.92	6.13	2.96	1.38	8.52
5.25	5.99	2.83	1.38	8.48
7.91	6.00	2.79	1.37	8.80
1.08×10^{8}	6.01	2.83	1.38	9.03
2.84	6.05	2.88	1.38	9.24
5.16	6.09	2.93	1.38	9.46
1.91×10^{9}	6.28	3.21	1.44	1.09×10^{2}
2.84	6.41	3.41	1.48	1.21
3.78	6.57	3.63	1.53	1.37
4.50	6.71	3.84	1.57	1.53

TABLE 4

Surface Characteristics of Models with $\frac{\ell}{H} = 1$

Age yrs.	$R/R_\odot$	$L/L_\odot$	log T_e	$\rho_{ph.}$ gm-cm^{-3}
3.17	60.86	330.7	3.502	1.50×10^{-8}
1.27×10	59.71	317.9	3.501	1.54
4.75	56.85	297.4	3.504	1.59
1.24×10^2	52.03	264.1	3.511	1.67
3.01	44.60	206.9	3.518	1.89
6.56	36.80	154.1	3.528	2.18
1.16×10^3	31.03	118.7	3.536	2.47
2.79	23.18	75.1	3.550	3.00
5.62	18.00	50.5	3.561	3.51
1.21×10^4	13.60	32.3	3.574	4.22
2.83	9.90	19.3	3.587	5.36
7.38	6.90	10.4	3.598	7.34
1.26×10^5	5.65	7.33	3.604	8.90
2.55	4.36	4.64	3.610	1.13×10^{-7}
6.71	3.13	2.38	3.610	1.69
1.09×10^6	2.67	1.75	3.611	2.00
1.92	2.22	1.20	3.611	2.50
3.58	1.82	0.80	3.609	3.22
5.24	1.61	0.62	3.609	3.73
8.56	2.39	0.47	3.611	4.32
1.19×10^7	1.28	0.42	3.617	4.47
1.85	1.17	0.46	3.644	3.72
2.19	1.17	0.54	3.663	3.04
3.18	1.17	0.99	3.726	1.78
3.35	1.15	0.99	3.732	1.72
3.52	1.11	0.95	3.736	1.73
4.51	0.98	0.72	3.732	2.06
5.84	0.97	0.69	3.730	2.11
8.41	0.97	0.71	3.731	2.08
1.14×10^8	0.98	0.72	3.733	2.05
2.94	0.98	0.73	3.733	2.03
5.33	0.99	0.74	3.733	2.00
7.73	1.00	0.76	3.734	1.98
1.01×10^9	1.00	0.77	3.734	1.96
2.21	1.04	0.83	3.734	1.88
3.17	1.07	0.90	3.737	1.78
4.13	1.11	0.96	3.737	1.71
4.50	1.11	0.99	3.739	1.66

TABLE 5

Surface Characteristics of Models with $\frac{\ell}{H} = 2$

Age yrs.	$R/R_\odot$	$L/L_\odot$	log T_e	$\rho_{ph.}$ gm-cm^{-3}
3.17	64.35	672.0	3.566	7.81×10^{-9}
1.27×10	62.34	643.5	3.568	7.89
3.72	58.20	576.9	3.571	8.21
1.13×10^2	49.84	464.1	3.581	8.63
2.15	43.40	369.2	3.586	9.51
6.20	32.13	230.8	3.600	1.12×10^{-8}
1.03×10^3	28.05	184.6	3.606	1.23
2.44	20.89	116.4	3.620	1.50
6.30	14.17	62.6	3.636	1.99
1.28×10^4	10.84	40.0	3.647	2.52
2.58	8.33	25.6	3.655	3.20
7.12	5.75	13.6	3.667	4.44
1.10×10^5	4.86	9.69	3.667	5.38
2.66	3.59	5.58	3.673	7.29
5.78	3.17	2.75	3.668	1.02×10^{-7}
1.82×10^6	1.89	1.26	3.650	1.95
2.65	1.69	0.96	3.645	2.37
4.31	1.48	0.71	3.641	2.91
7.64	1.28	0.54	3.642	3.44
1.43×10^7	1.11	0.51	3.668	3.06
2.09	1.04	0.69	3.714	2.23
2.76	1.00	0.96	3.760	1.56
2.92	0.99	1.00	3.767	1.44
3.26	0.93	0.89	3.766	1.56
3.92	0.88	0.76	3.761	1.77
5.25	0.86	0.73	3.761	1.82
7.91	0.86	0.71	3.759	1.78
1.08×10^8	0.86	0.72	3.760	1.83
2.83	0.87	0.74	3.761	1.80
5.16	0.88	0.75	3.761	1.78
1.91×10^9	0.90	0.82	3.764	1.66
2.84	0.92	0.88	3.766	1.57
3.78	0.95	0.93	3.768	1.49
4.50	0.97	0.99	3.770	1.42

in solar units and the corresponding effective temperatures Te and photospheric densities ρ_{ph} for $\frac{\ell}{H}$ = 1 and 2, respectively. The positions of the models in the Hertzsprung-Russell d gram are shown in Figure 2.

The evolutionary track calculated with $\frac{\ell}{H}$ = 2 resulted in bringing the sun nearly to the right position in the Hertzsprung-Russell diagram at the end of 4.5 x 10^9 years. Since the purpose of this investigation is not to obtain a perfect model of the present sun, no further attempt has been made to improve the resulting radius and luminosity by adjusting the initial solar composition and the assumed mixing-length ratio. Therefore $\frac{\ell}{H}$ = 2 is used in order to explore further characteristics of the evolution of the sun. In Figure 3, the calculated track with $\frac{\ell}{H}$ = 2 and corresponding evolution times have been shown. In the following, all discussions relate to the results obtained with $\frac{\ell}{H}$ = 2.

Under the assumption that the sun possesses no angular momentum, it becomes stable against gravitational collapse when it contracts to a radius of 64 $R_\odot$. Its initial luminosity is about 693 times the luminosity of the present sun. It stays fully convective until it has contracted to a radius of 2 $R_\odot$. By then, its luminosity has been reduced

to 1.5 $L_\odot$; with the increase of central temperature and density through the contraction, a radiative core starts to develop. The luminosity keeps decreasing as long as, in the main part of the sun, the energy is transferred by convective motions of the gases. The luminosity reaches a minimum value $L = 0.512\ L_\odot$ at the end of 1.4×10^7 years. At that time 58% of the radius and 75% of the mass of the sun have been covered by the radiative core. With further evolution, the radiative region continuously extends toward the surface and the sun follows an evolutionary path which is determined by radiative equilibrium. In Figure 4 the change of the internal structure and luminosity of the sun with time have been shown. The physical characteristics of these partly convective models are indicated in Table 6a and Table 6b. The first column gives the evolution time in years, the second and third columns give the luminosity and radius of the model, and the fourth, fifth and sixth columns give the temperature, density and the mass fraction inside the core.

In Figure 4 the curves indicated by X_3 and X_{12} give the change of the abundances, by mass, of He^3 and C^{12} at the center of the sun. He^3 begins to form at the central temperature 7×10^6 °K and central density 20 gm/cm^3 after 1.43×10^7 years. It reaches local equilibrium values near the center of the sun in about 1.5×10^7 years, at a temperature of about 1.3×10^7 °K. Around the temperature of 1.2×10^7 °K, C^{12} also begins to burn. The energy generated

TABLE 6a

Some Physical Characteristics at the Base of Convective Region ($\frac{\ell}{H} = 2$)

Age yrs.	L erg sec^{-1}	R cm	T °K b. conv.	ρ gm cm^{-3} b. conv.	(M_r/M) b. conv.
1.82×10^6	4.90×10^{33}	1.31×10^{11}	3.62×10^6	1.13	0.04
2.65	3.74	1.17	3.53	1.27	0.17
4.31	2.77	1.03	3.42	1.45	0.32
7.64	2.09	8.92	3.21	1.47	0.54
1.43×10^7	2.00	7.72	3.04	1.17	0.77
2.09	2.71	7.26	2.47	0.43	0.94
2.76	3.74	6.94	2.15	0.23	0.98
5.25	2.83	5.99	1.92	0.18	0.99

TABLE 6b

Some Physical Characteristics at the Surface of Central Convective Region ($\frac{\ell}{H}=2$)

Age yrs.	L erg sec^{-1}	R cm	T °K s. ce. conv.	ρ gm cm^{-3} s. ce.conv.	(M_r/M) s. ce. conv.
2.92×10^7	3.92×10^{33}	6.85×10^{10}	1.18×10^7	79.9	0.03
3.26	3.47	6.49	1.15	68.4	0.09
5.25	2.83	5.99	1.18	68.0	0.07
1.08×10^8	2.83	6.01	1.25	78.4	0.03
2.83	2.88	6.05	1.28	83.2	0.02
5.16	2.93	6.09	1.30	86.6	0.01
1.91×10^9	3.21	6.28	1.37	102.1	.007
2.84	3.41	6.41	1.43	114.8	.004
3.78	3.63	6.57	1.49	131.3	.002
4.50	3.84	6.71	1.53	147.5	.001

by nuclear burning supplements the energy contribution from gravitational contraction to the total luminosity of the sun. The luminosity reaches its local peak value prior to settling onto the main sequence whereupon the centrally condensed nuclear energy sources entirely supply the energy output of the sun. A high rate of energy generation, due to sudden nuclear burning, causes the development of a convective core at the center of the sun. With the development of the convective core, the He^3 abundance at the center of the sun suddenly decreases due to the fact that He^3 has still not reached its local equilibrium value at the regions far from the center, but the convective motion of the gases brings He^3 into average equilibrium throughout the convective zone. This convective core extends over about 9% of the mass. The luminosity decreases and attains its final minimum value before the main sequence, while the convective core extends to its maximum size. After C^{12} is depleted by a sufficient amount, this convective core diminishes in size, and, at the end of 4.5×10^9 years, covers only 0.1% of the mass.

In Figure 5 the distribution of luminosity (L_r/L), the nuclear (ϵ_N) and gravitational (ϵ_g) energies, and the He^3 abundance by mass (X_3) are given as a function of mass fraction throughout the interior of the sun, at the time when the sun reaches its local maximum luminosity near the main sequence. The scaling factors for the quantities are $L = 3.916 \times 10^{33}$ erg/sec, $\epsilon_N = \epsilon_g = 25.70$ erg/gm-sec,

and $X_3 = 1.724 \times 10^{-4}$. He^3 is still building up toward its equilibrium value throughout the interior of the sun. The gravitational energy becomes negative due to the expansion of inner layers while the central convective core is developing. The outer layers are still contracting.

In Figure 6 the same quantities (except ϵ_g), together with the abundance of C^{12} by mass (X_{12}),(scaled by 4.618×10^{-3}), are indicated for the model at which the luminosity of the sun has its local minimum, i.e. "zero-age"main sequence. In the core He^3 is in steady-state equilibrium. Outside the core it is in local equilibrium up to the mass fraction 0.14, and further out it is still building up toward its equilibrium value. C^{12} has been reduced substantially, but still has not reached its equilibrium value inside the sun. In Table 7, values of the physical variables within the model of the present sun, obtained at the end of 4.5×10^9 years, are tabulated.

The calculations were also carried out on the assumption that the contracting solar material contains the terrestrial ratio of deuterium to hydrogen and some initial He^3. When the sun contracts to a radius of about 10 $R_\odot$ the central temperature is in the vicinity of 800,000 ^oK. At these temperatures, deuterium will burn through the $H^2(p,\gamma)He^3$ reaction; since the sun is fully convective, the material is throughly mixed inside the sun and all deterium will be completely burned. While deuterium is burning, the gravitational contraction stops, and the energy

TABLE 7

Physical Variables in the Present Sun

M_r/M	$r \times 10^{-10}$ cm	ρ gm cm^{-3}	$P \times 10^{-15}$ dy cm^{-2}	$T \times 10^{-6}$ °K	$L_r \times 10^{-33}$ erg sec^{-1}	X_1
0.00	0.0	153	256	15.7	0.00	.409
0.02	0.41	126	202	14.4	0.62	.478
0.04	0.53	109	178	13.8	1.10	.527
0.06	0.63	98.3	160	13.3	1.51	.562
0.08	0.70	89.9	145	12.9	1.85	.589
0.10	0.77	83.0	132	12.5	2.14	.612
0.12	0.83	77.1	121	12.1	2.38	.630
0.14	0.89	71.8	111	11.8	2.60	.645
0.16	0.94	67.1	102	11.5	2.78	.656
0.18	0.99	62.8	94.1	11.2	2.94	.669
0.20	1.04	58.9	86.8	11.0	3.08	.678
0.30	1.28	43.3	58.0	9.74	3.52	.710
0.40	1.50	31.6	38.1	8.69	3.72	.725
0.50	1.73	22.3	24.2	7.74	3.81	.732
0.60	1.98	14.9	14.3	6.84	3.84	.736
0.70	2.28	9.05	7.52	5.94	3.84	.738
0.80	2.68	4.61	3.22	4.99	3.85	.739
0.90	3.32	1.56	.837	3.85	3.85	.739
1.00	6.71	0.00	0.000	0.00	3.85	.739

generated by the deuterium burning completely suffices to supply the energy losses of the sun. The deuterium burning extends the evolution time by about 520,000 years. Due to the He^3 initially present, the sun comes into nuclear-burning equilibrium earlier. The evolutionary track differs only slightly from the one with no initial He^3.

The problem of lithium abundances in the present sun has also been considered. The observed abundance of lithium in the sun is much smaller than is found for the earth and meteorites. Lithium will be found as two stable isotopes in the solar material: Li^6 and Li^7. Assuming that the mixing of the material is rapid enough to keep it homogeneous inside the convective region, we can calculate the relative number of lithium nuclei which have been destroyed in the sun from the relation

$$\frac{d\ \ell n\ n}{dt} = \frac{\int_{M_{b\ conv.}}^{1} p\ dM}{M_{conv.}}$$

where n is the abundance of the lithium isotope in question, p is the reaction rate and $M_{b\ conv.}$ is the mass fraction at the bottom of the convective region. The reaction rate for the $Li^6(p,\alpha)He^3$ reaction per nucleus per second is (Reeves, 1963)

$$\frac{p}{\rho X_1} = 5.96 \times 10^{12} \frac{e^{-84.149/T_6^{1/3}}}{T_6^{2/3}}$$

and that for the $Li^7(p,\alpha)He^4$ reaction is (Reeves, 1963)

$$\frac{p}{\rho X_1} = 1.20 \times 10 \frac{e^{-84.731/T_6^{1/3}}}{T_6^{2/3}}$$

In Figure 7, the rate of lithium burning versus time has been indicated for two different mixing-length ratios. The maximum rate of burning occurred around an evolution time of 3.5×10^6 years. It has been found that the depletion of Li^6 is complete, but Li^7 is depleted by factors of 1.5 for the mixing-lengths equal to two pressure scale heights. The above calculations have been performed on the assumption that penetrative convection and internal circulation currents play no role.

The neutrino fluxes at 1 astronomical unit from the sun have been estimated by using the last model representing the present sun at the end of 4.5×10^9 years.

The rate of neturino emission per gram has been integrated through this model taking into account the various nuclear reaction rates in the interior. The neutrino fluxes from the $H^1(p,\beta^+\nu)D^2$, $Be^7(e^-,\nu)Li^7$, $B^8(\beta^+\nu)Be^8$, $N^{13}(\beta^+\nu)C^{13}$ and $O^{15}(\beta^+\nu)N^{15}$ reactions (since the CN cycle is not assumed in equilibrium) are shown in Table 8.

Table 8

Neutrino Fluxes at 1 Astronomical Unit ($cm^{-2}sec^{-1}$)

	ν_H	ν_{Be}	ν_B	ν_N	ν_O
Ours	5.91×10^{10}	0.69×10^{10}	0.95×10^{7}	0.60×10^{9}	0.51×10^{9}
Sears	5.80×10^{10}	0.82×10^{10}	1.90×10^{7}	0.48×10^{9}	

In Table 8 the neutrino fluxes calculated by Sears (1964) are also given. They were obtained from his best model, which is nearly consistent with the available data for the sun. We have lower values for neutrinos from beryllium-7 and boron-8. The neutrino flux which reaches the earth is about 6.65×10^{10} neutrinos per square centimeter per second. This is compatible with the resulting luminosity of our model for the present sun.

The high luminosity of the initial evolutionary phase of the sun only lasts about 10^6 years. The time required to reach the main sequence, defined as the point at which the sun's luminosity has its final minimum value before the main hydrogen burning starts, is about 7.5×10^7 years for the sun.

The resulting luminosity for the present sun is 3.84×10^{33} erg-sec^{-1}, which is very close to the observed value. This indicates that our initial composition is the proper one for the solar material. The calculated radius is three percent smaller than the observed radius. This can be explained by our choice of two pressure scale heights for the mixing length; a little smaller value might give a more realistic value for the radius of the sun.

ACKNOWLEDGEMENTS

One of us (D. Ezer) would like to express her thanks to Dr. Henyey for his generous help and discussion in setting up the Henyey method. The authors are also very grateful to Mr. Bernard Sackaroff for his assistance in programming and carrying out the calculations.

One of us (D. Ezer) would like to express her appreciation to Dr. Robert Jastrow for the hospitality of the Institute for Space Studies and to the National Academy of Sciences - National Research Council for the associateship under which the main part of this work was carried out.

REFERENCES

Aller, L.H. 1963. Astrophysics, I, The atmosphere of the sun and stars, (Ronald Press, New York).

Bahcall, J.N. 1962. Phys. Rev. 128, 1297.

Biswas, S., Fichtel, C.E., Guss, D.E., and Waddington, C.J. 1963. J. Geophys. Res. 68, 3109.

Cameron, A.G.W. 1962. Icarus, 1, 13.

Cox, A.N. 1964. Stellar absorption coefficients and opacities in "Stellar Interiors," ed. by L.H. Aller and D.B. McLaughlin (Univ. of Chicago Press, Chicago, in press).

Ezer, D. and Cameron, A.G.W. 1963. Icarus, 1, 422.

Ezer, D. and Cameron, A.G.W. 1964. Evolution in the contraction phase, in "Stellar Evolution," ed. by R.F. Stein and A.G.W. Cameron (J. Wiley and Sons, New York, (in press).

Gaustad, J.E. 1964. Astrophys. J., 139, 406.

Hayashi, C. 1961. Publ. Astron. Soc. Japan, 13, 450.

Henyey, L.G., Forbes, J.E., and Gould, N.L. 1964. Astrophys. J., 139, 306.

Hofmeister, E., Kippenhahn, R., and Weigert, A. 1964. Zeits. f. Astrophys. 59, 215.

Reeves, H. 1963. Stellar energy sources, in "Stars and Stellar Systems," vol. VIII, ed. by L.H. Aller and D.B. McLaughlin (Univ. of Chicago Press, Chicago, in press).

Sears, R.L. 1964. Astrophys. J., 140, 477.

Vitense, E.B. 1958. Zeits. f. Astrophys., 46, 108.

Weymann, R. and Moore, E. 1963. Astrophys. J., 137, 552.

at several positions.

Figure 4: The change of the internal structure and luminosity of the sun with time. The Sun ceases to be fully convective after 1.4 million years. A small convective core developes at the evolution time 2.9 x 10^7 years. The curves X_3 and X_{12} show the variation with time of the abundances, by mass, of He^3 and C^{12} at the center of the sun.

Figure 5: The variation of the luminosity (L_r/L), the nuclear (ϵ_N) and gravitational (ϵ_g) energies, and He^3 abundance by mass (X_3) as a function of mass fraction, at the stage where the sun reaches its local maximum value near the main sequence.

Figure 6: The variation of the luminosity (L_r/L), nuclear energy (ϵN_{12}), and the abundances by mass of He^3 (X_3) and C^{12} (X_{12}) inside the sun at the stage for which the luminosity of the sun has its local minimum; i.e. the "zero-age" main sequence model.

Figure 7: The rate of lithium burning for both isotopes of lithium versus their evolution time. The rate of burning is higher for the mixing-length, equal to two pressure scale heights.

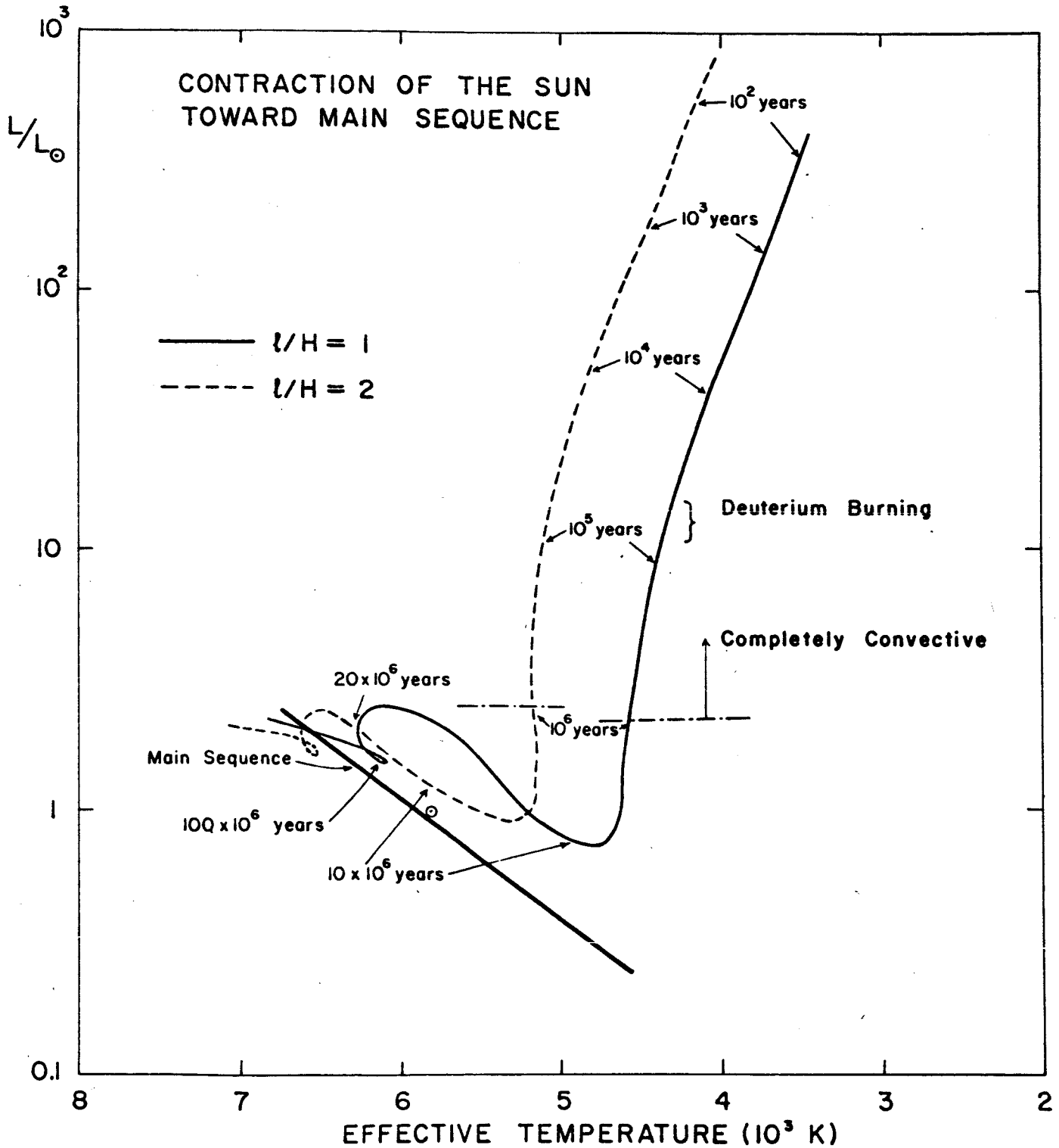
CONTRACTION OF THE SUN
TOWARD MAIN SEQUENCE
L/L⊙
10^3
10^2
10
1
0.1
ℓ/H = 1
ℓ/H = 2
10^2 years
10^3 years
10^4 years
10^5 years
Deuterium Burning
Completely Convective
20 x 10^6 years
10^6 years
Main Sequence
100 x 10^6 years
10 x 10^6 years
8
7
6
5
4
3
2
EFFECTIVE TEMPERATURE (10^3 K)

Fig. 1

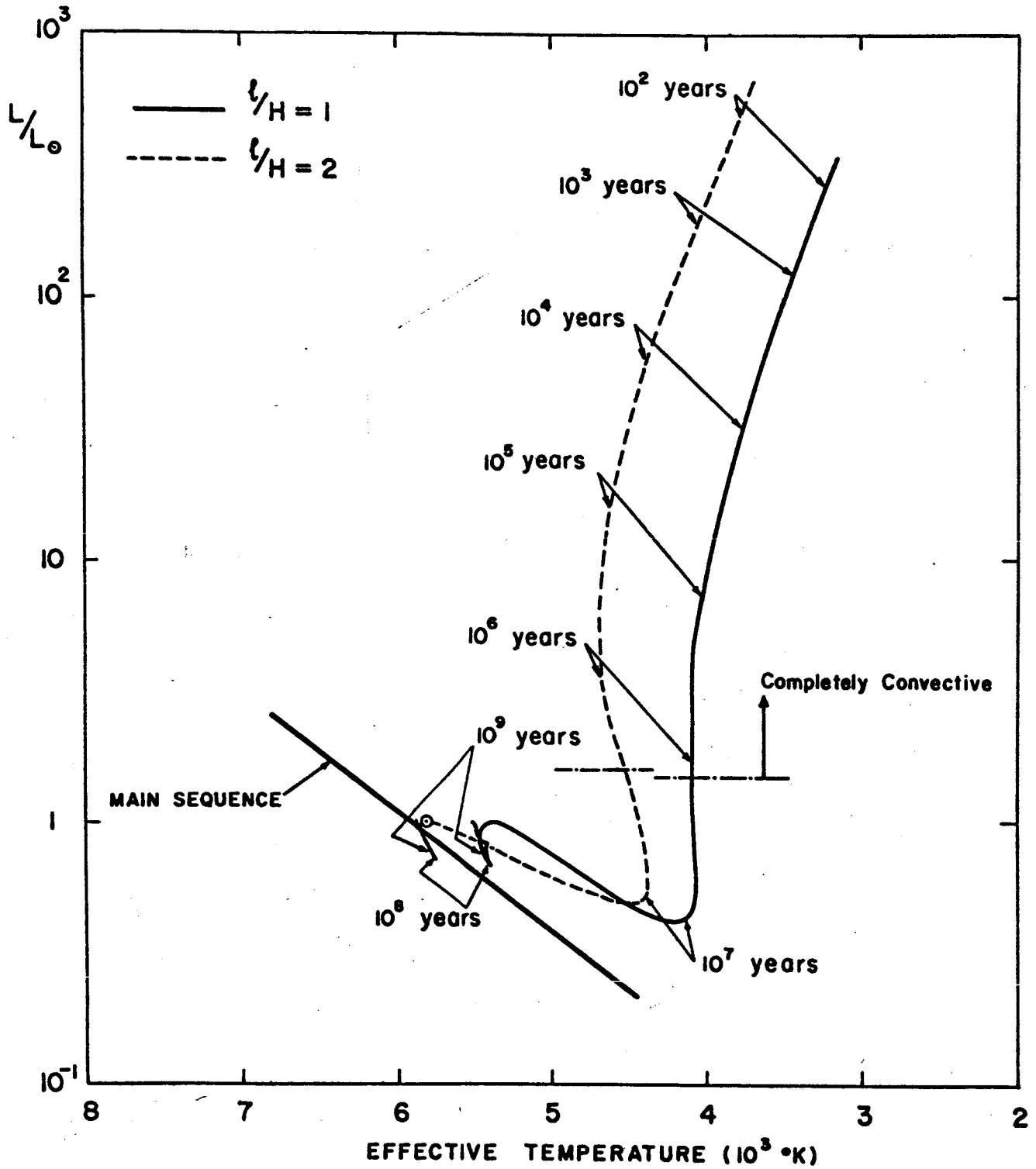
10^3
$L/L_\odot$
$\ell/H = 1$
$\ell/H = 2$
10^2 years
10^3 years
10^4 years
10^5 years
10^6 years
Completely Convective
10^9 years
MAIN SEQUENCE
10^8 years
10^7 years
10^2
10
1
10^{-1}
8
7
6
5
4
3
2
EFFECTIVE TEMPERATURE (10^3 °K)

Fig. 2

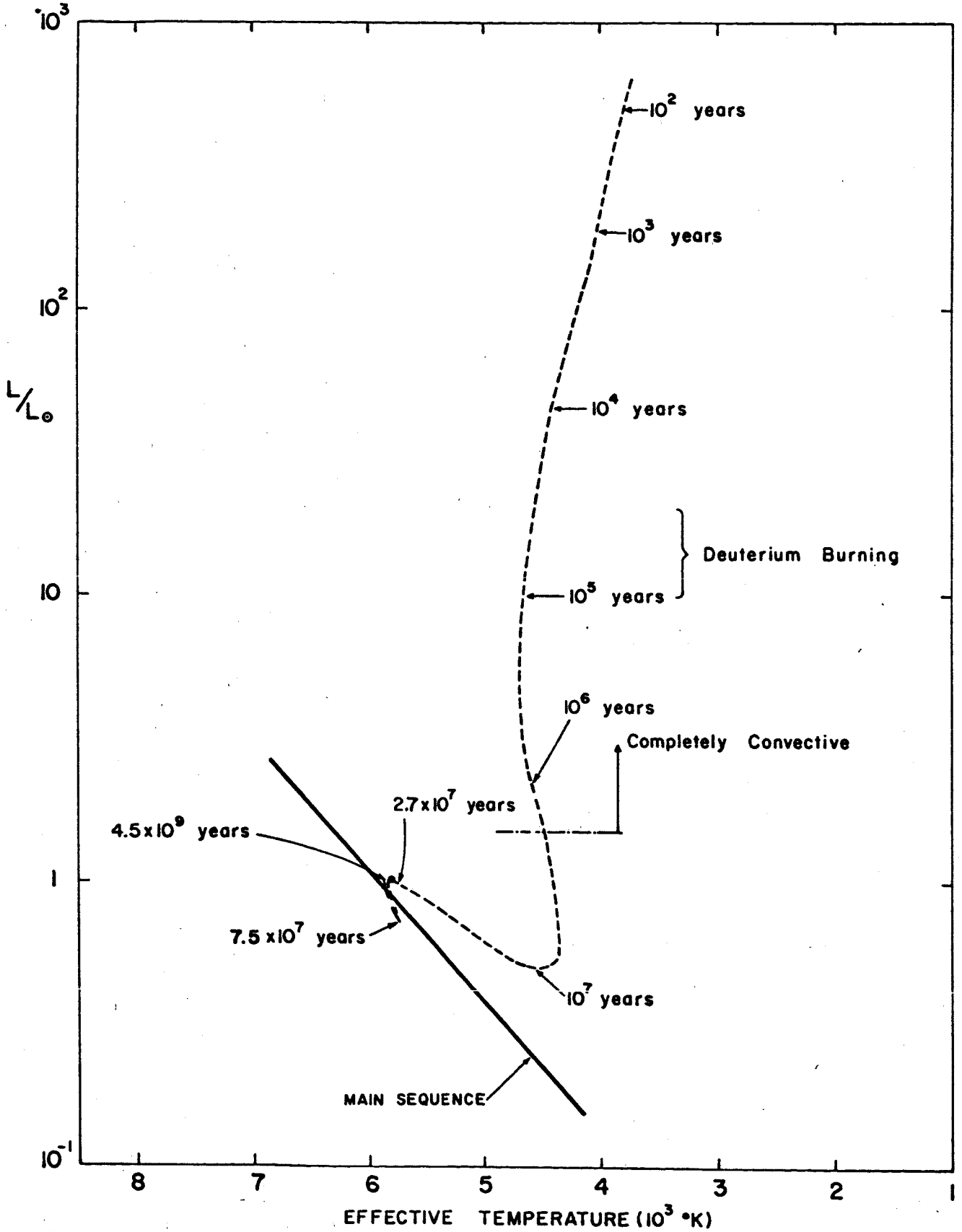
10^3
10^2
10
1
10^{-1}
$L/L_\odot$
10^2 years
10^3 years
10^4 years
Deuterium Burning
10^5 years
10^6 years
Completely Convective
2.7×10^7 years
4.5×10^9 years
7.5×10^7 years
10^7 years
MAIN SEQUENCE
8
7
6
5
4
3
2
1
EFFECTIVE TEMPERATURE (10^3 °K)

Fig. 3

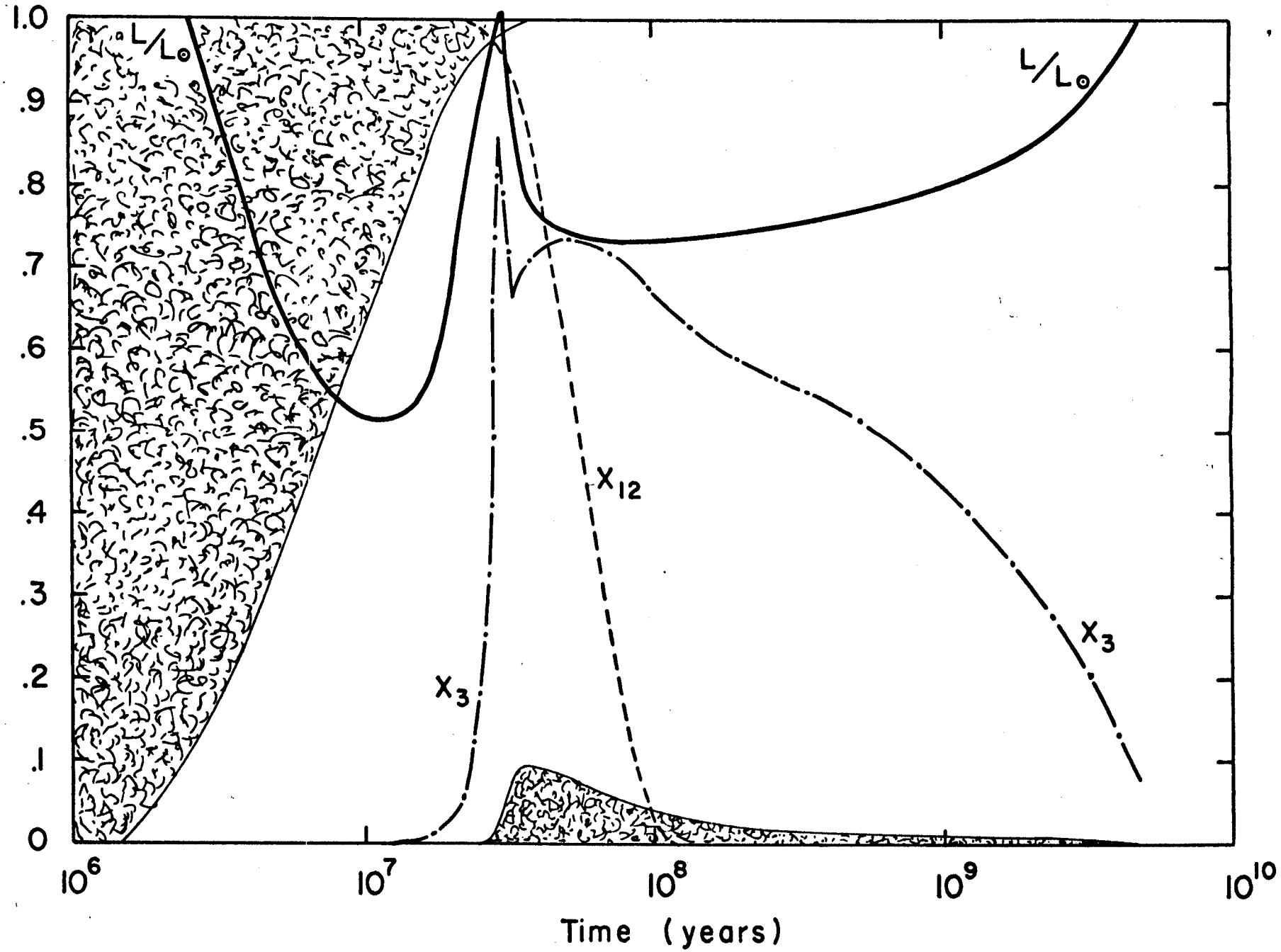

Fig. 4

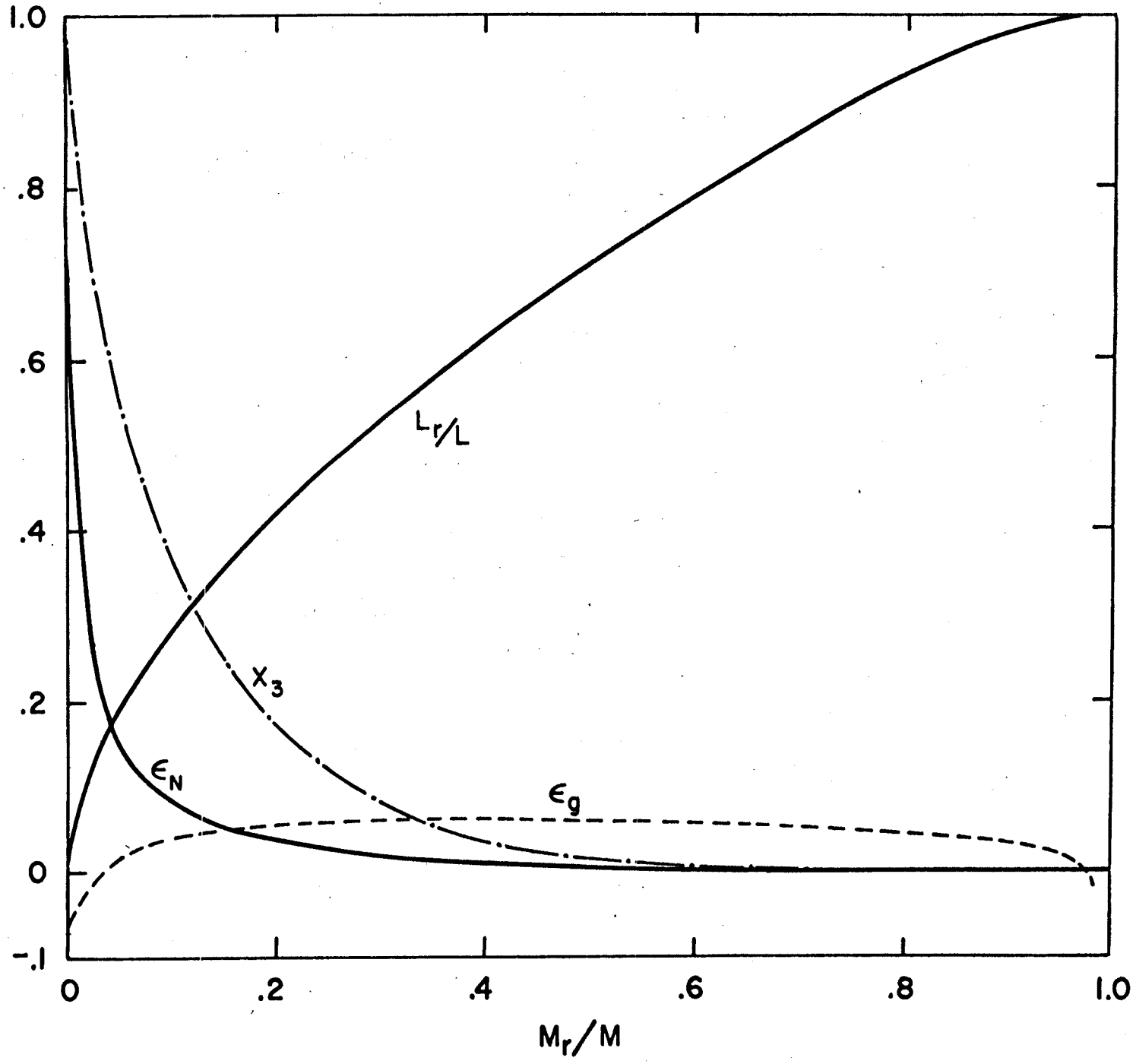

Fig. 5

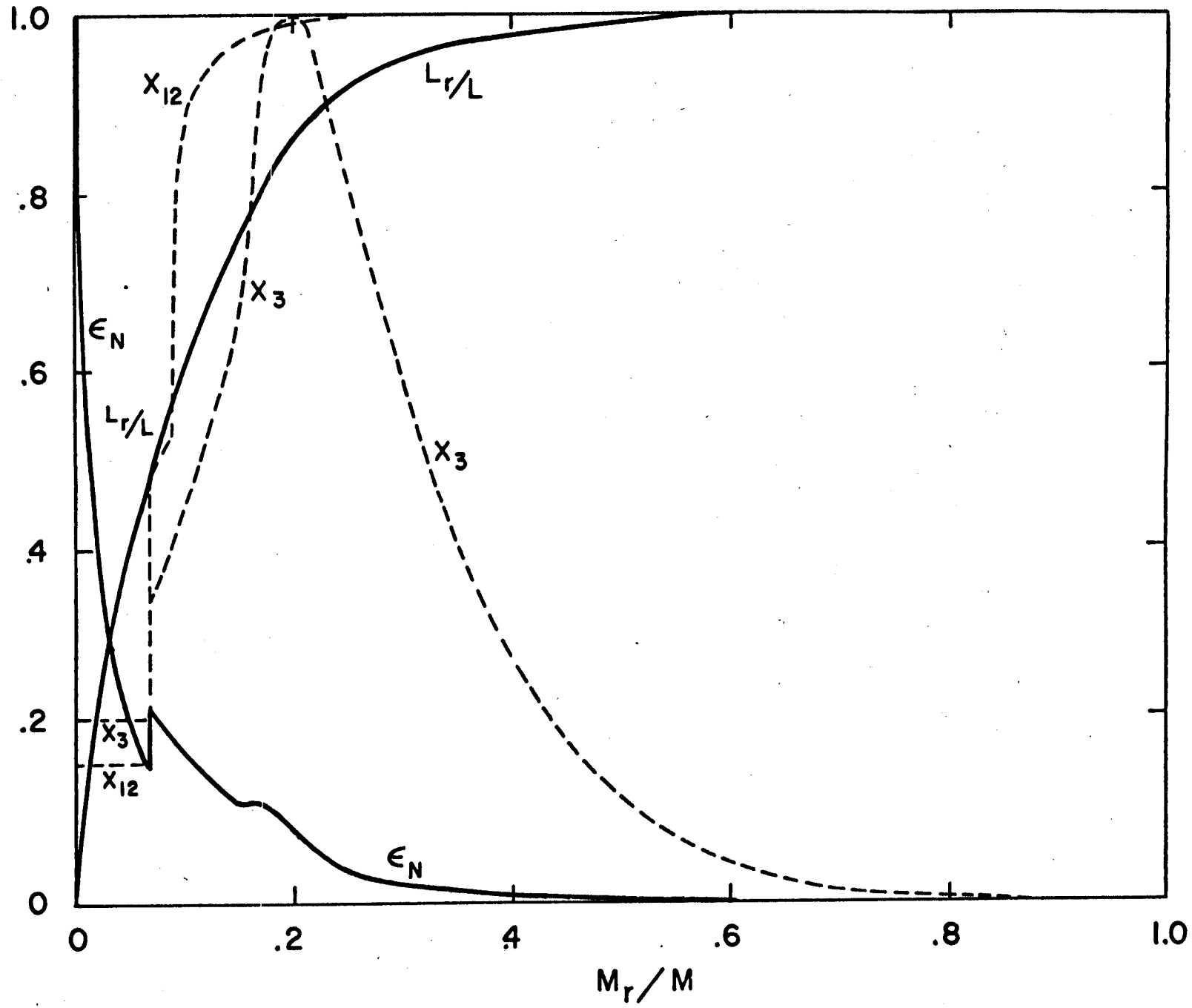
1.0
.8
.6
.4
.2
0
0
.2
.4
.6
.8
1.0
M_r/M
X_{12}
L_r/L
X_3
ϵ_N
L_r/L
X_3
ϵ_N
$\bar{X}_3$
$\bar{X}_{12}$

Fig. 6

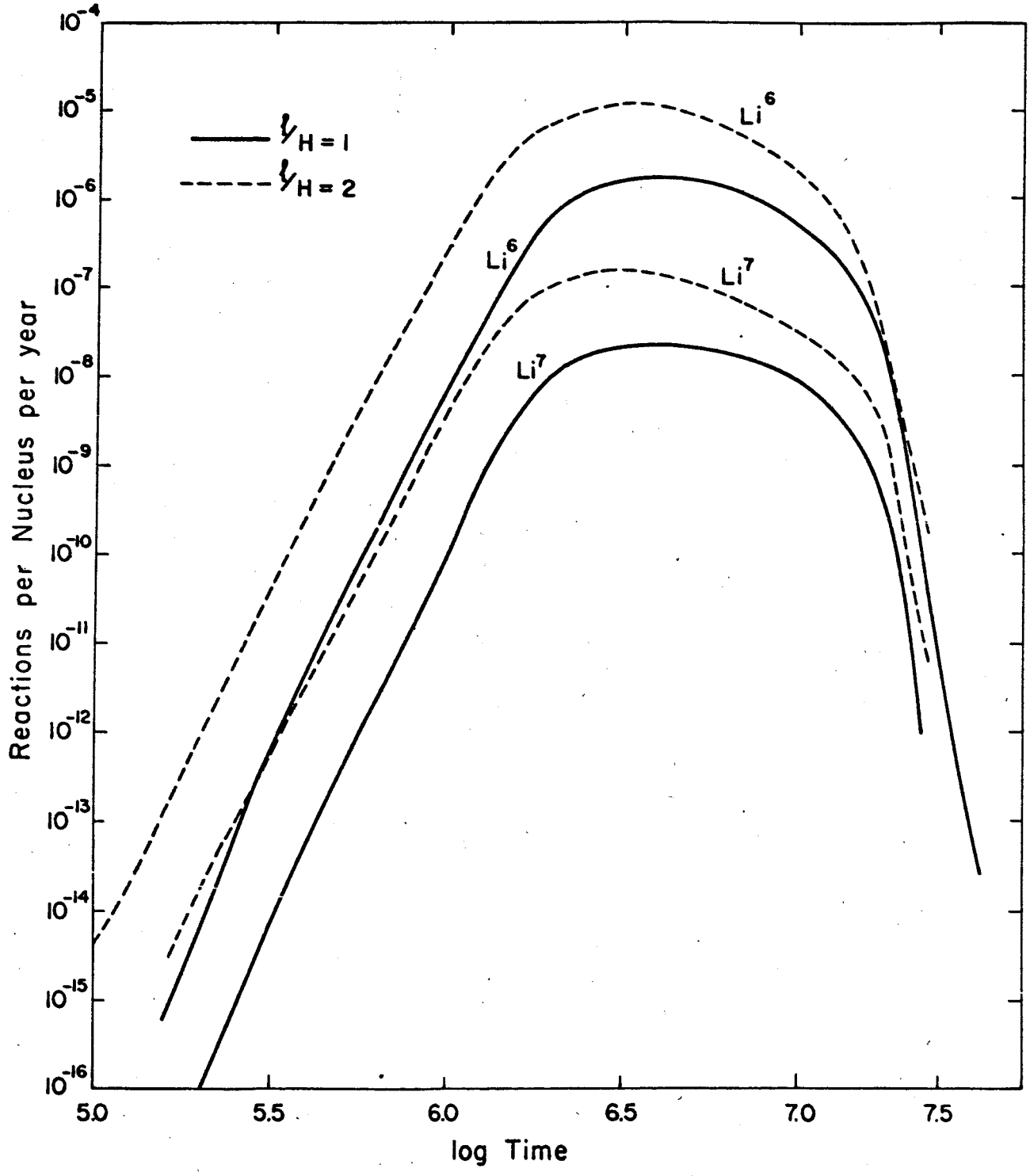

Fig. 7

GPO 950-100